ORIGINAL ARTICLE

Enhanced solar radiation pressure modeling for Galileo satellites

O. Montenbruck · P. Steigenberger · U. Hugentobler

Abstract This paper introduces a new approach for modeling solar radiation pressure (SRP) effects on Global Navigation Satellite Systems (GNSSs). It focuses on the Galileo In-Orbit Validation (IOV) satellites, for which obvious SRP modeling deficits can be identified in presently available precise orbit products. To overcome these problems, the estimation of empirical accelerations in the Sun direction (D), solar panel axis (Y) and the orthogonal (B) axis is complemented by an a priori model accounting for the contribution of the rectangular spacecraft body. Other than the GPS satellites, which comprise an almost cubic body, the Galileo IOV satellites exhibit a notably rectangular shape with a ratio of about 2:1 for the main body axes. Use of the a priori box model allows to properly model the varying cross section exposed to the Sun during yaw-steering attitude mode and helps to remove systematic once-per-revolution orbit errors that have so far affected the Galileo orbit determination. Parameters of a simple a priori cuboid model suitable for the IOV satellites are established from the analysis of a long-term set of GNSS observations collected with the global network of the Multi-GNSS Experiment of the International GNSS Service. The model is finally demonstrated to reduce the peak magnitude of radial orbit errors from presently 20 cm down to 5 cm outside eclipse phases.

O. Montenbruck (✉) · P. Steigenberger
German Space Operations Center, Deutsches Zentrum
für Luft- und Raumfahrt, 82230 Weßling, Germany
e-mail: oliver.montenbruck@dlr.de

U. Hugentobler
Institut für Astronomische und Physikalische Geodäsie,
Technische Universität München, 80290 München, Germany

1 Introduction

As part of the preparation and build-up of Europe's global navigation satellite system (GNSS) Galileo, a total of six satellites has been launched between December 2005 and October 2012. Within the Galileo In-Orbit Validation Element (GIOVE) the first two satellites (GIOVE-A/B) served to secure the Galileo frequencies and to flight-test critical technology components (Binda and Fletcher 2011). Among others, these included a Rubidium Atomic Frequency Standard (RAFS) and the first Passive Hydrogen Maser (PHM) flown on a navigation satellite. The four subsequent In-Orbit Validation (IOV) satellites initiated the build-up of the full Galileo constellation and will ultimately become part of the operational system.

Precise orbit determination (POD) of the GIOVE and IOV satellites has been a key goal of both the Galileo project and the scientific community to assess, demonstrate and improve the achievable navigation performance and to characterize the stability of the various onboard clocks. Since all of the aforementioned satellites are equipped with laser retroreflector arrays (LRAs), satellite laser ranging (SLR) measurements collected by the International Laser Ranging Service (ILRS; Pearlman et al. 2002) can be used to independently assess the quality of GNSS-based POD solutions. Early results for GIOVE-A and -B are described in Schönemann et al. (2007) and Steigenberger et al. (2011) where accuracies at the few decimeter level are achieved. Waller et al. (2010) report clock variations with a 1/rev signature for both GIOVE satellites. While these can be clearly related to thermal changes for GIOVE-A, orbit modeling errors are suspected in case of GIOVE-B. This assumption is further substantiated by Svehla et al. (2010), who first demonstrate the correlation of periodic clock variations and SLR residuals for GIOVE-B. In their comparative study of GIOVE-B and the

first GPS Block IIF satellite, Montenbruck et al. (2012) highlight the distinct impact of orbit errors and thermal variations on the observed clock and demonstrate a beneficial impact of a combined GNSS + SLR processing on the GIOVE-B orbit determination performance. Hackel et al. (2014) later extend that work to the first two Galileo IOV satellites, for which an orbit accuracy of 1 dm is achieved on average. Most recently, a comprehensive comparison of Galileo IOV orbit determination solutions obtained within the Multi-GNSS Experiment (MGEX) of the International GNSS Service (IGS; Dow et al. 2009) has demonstrated a precision of about 1 dm (3D rms) and a radial accuracy of better than 20 cm (Steigenberger et al. 2014).

The limited performance of early GIOVE and Galileo IOV orbit products in comparison to those of GPS has initially been attributed to limitation of the employed monitoring network, the lacking application of integer ambiguity resolution, or the unavailability of proper antenna offset and phase pattern information. An evidence of solar radiation pressure (SRP) modeling deficiencies was first obtained in a long-term analysis of satellite laser ranging residuals for all four Galileo IOV satellites (Montenbruck et al. 2013). Here, it could be shown that the amplitude of 1/rev radial orbit errors in the GNSS-only orbit solutions varies with the Sun elevation above the orbital plane (β-angle). It is smallest for high elevations, but increases to roughly 20 cm near the eclipse season. Furthermore, the authors demonstrated that the radial orbit errors at any epoch can be described by a function of the Sun elongation (i.e., the angle ε between the Earth and Sun direction as seen from the GNSS satellite). Building up on this finding, Steigenberger et al. (2014) were later able to obtain an empirical clock correction and to place a new upper limit on the Allan deviation of the IOV satellites at orbital time scales.

In the absence of a detailed, physics-based SRP model for the Galileo satellites, the POD studies quoted above have typically made use of an empirical SRP model. The CODE model (named after the Center for Orbit Determination in Europe that first established its use for GPS; Beutler et al. 1994) allows for the adjustment of constant and orbit-periodic accelerations along three orthogonal axes aligned with the Sun and solar panel direction.

Within the present study, different concepts for SRP modeling of GPS and GLONASS satellites are first revisited along with the basic properties of yaw-steering attitude control (Sect. 2). The performance of the CODE SRP model for orbit determination of the Galileo satellites is examined in Sect. 3 and the failure of this model to properly describe the motion of the Galileo satellites is traced to the shape properties of the satellite body. Based on this result, an a priori box model augmenting the standard CODE model is established for the Galileo satellites and its parameters are adjusted based on Galileo observations covering the full range of Sun ele-
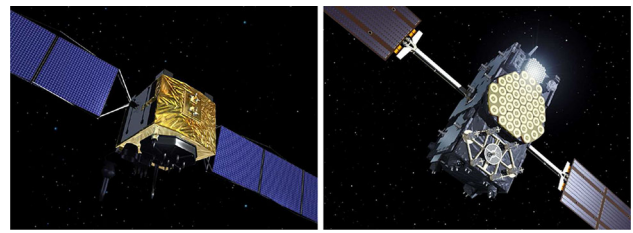
Fig. 1 Artist's impression of the GPS Block IIF (*left* ©Boeing) and Galileo IOV (*right* ©ESA) satellites

vations (Sect. 4). Finally, the combined model is applied to 6 months of Galileo observations to demonstrate the benefits for orbit (and clock) determination (Sect. 5).

The study focuses on the SRP modeling of the Galileo IOV satellites, which exhibit a notably non-cubic spacecraft body compared to present GPS satellites (Fig. 1). Other than GIOVE-A and -B, the IOV satellites have been tracked by a sufficiently large number of GNSS monitoring stations. Furthermore, all IOV spacecraft are equipped with PHM frequency standards that lend themselves for an independent validation of SRP-induced orbit errors.

2 SRP models for GNSS satellites

Next to the gravitational attraction of the Earth, Moon, and Sun, SRP constitutes the dominating source of acceleration acting on GNSS satellites (Milani et al. 1987). At a representative magnitude of 100 nm/s^2, it introduces orbital perturbations at the level of 100 m over time scales of one orbital revolution (Beutler 2005; Fliegel and Gallini 1996). SRP depends on the optical properties of the reflecting surface and its orientation with respect to the incident radiation. The relevant reference frames are therefore described in Sect. 2.1. Depending on the employed concepts, analytical and empirical SRP models may be distinguished. While the former aim at physical description of the net force resulting from the absorbed and reflected radiation (Sect. 2.2), the latter introduce a properly chosen combination of empirical accelerations that are adjusted along with other parameters in the orbit determination process (Sect. 2.3).

2.1 Yaw-Steering attitude control

With the exception of eclipse phases and geostationary orbits, GNSS satellites are traditionally operated in a yaw-steering attitude mode (Konrad et al. 2007). Here, the spacecraft is continuously rotated about the Earth-pointing antenna boresight axis such that the solar panel rotation axis is always perpendicular to both the Earth and Sun direction (Fig. 2). In this way, the solar panel normal vector can be adjusted towards the Sun at all times to maximize the collected energy. With-
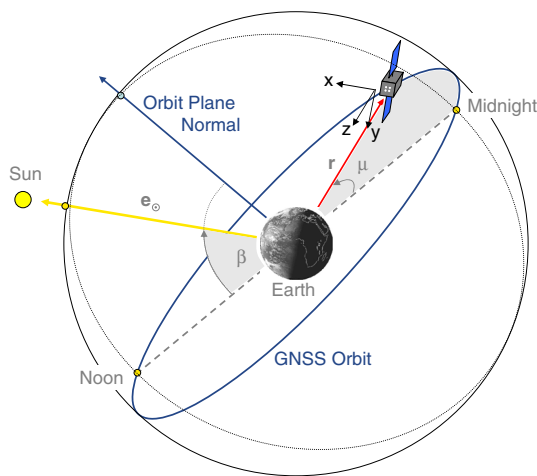
Fig. 2 Yaw-steering attitude control of GNSS satellites

out loss of generality, we adopt the IGS naming convention (Kouba and Héroux 2001) for the individual axes of the right-handed x, y, and z spacecraft coordinate system. Here, $+z$ designates the axis which holds the transmit antenna and is nominally Earth pointing, the solar panels are mounted in the $\pm y$-axis and the $+x$-axis points into the hemisphere containing the Sun. Even though manufacturer-specific axis labels may be differently chosen, the above convention facilitates a common description of attitude laws for different constellations. Making use of the satellite position vector r and the Sun direction unit vector $e_\odot$, the spacecraft orientation in yaw-steering mode is described by the three unit vectors

$$e_z = -\frac{r}{|r|}$$
$$e_y = \frac{e_z \times e_\odot}{|e_z \times e_\odot|}$$
$$e_x = e_y \times e_z. \tag{1}$$

Assuming a perfect yaw-steering and solar panel orientation, the solar pressure-induced accelerations are confined to the xz-plane and depend only on the Sun–spacecraft–Earth angle, or elongation, $\varepsilon = \angle(e_z, e_\odot)$. At Sun elevation β and orbit angle μ (see Fig. 2), the elongation is given by

$$\cos \varepsilon = \cos \beta \cos \mu \tag{2}$$

(Bar-Sever 1996). It varies between a minimum of β at local midnight ($\mu = 0$) and a maximum of $\pi - \beta$ at local noon ($\mu = \pi$).

2.2 Analytical SRP models

Solar radiation pressure results from the impulse transfer of absorbed and emitted photons on a surface illuminated by the Sun. For describing the radiation pressure force, we consider a single flat surface element of area A that is subject to an incident flux Φ. The surface normal and the direction of the illuminating source are described by the unit vectors e_n and $e_\odot$, which enclose an angle

$$\theta = \arccos(e_\odot^T e_n) > 0. \tag{3}$$

The solar flux in the vicinity of the Earth amounts to

$$\Phi = 1{,}367 \text{ W/m}^2 \cdot \frac{1 \text{ AU}^2}{r_\odot^2}, \tag{4}$$

where $r_\odot$ denotes the instantaneous distance of the satellite from the Sun and where the astronomical unit (1 AU = 149.6×10^6 km) describes the mean Sun–Earth distance. Given the fractions α, δ, and ρ (with $\alpha + \delta + \rho = 1$) of absorbed as well as diffusely and specularly reflected photons (Milani et al. 1987), the resulting net force F is given by

$$F = -\frac{\Phi}{c} \cdot A \cos \theta \cdot \left[(\alpha + \delta)e_\odot + \frac{2}{3}\delta e_n + 2\rho \cos \theta \cdot e_n \right]. \tag{5}$$

Assuming that the absorbed radiation is instantaneously re-radiated in accord with Lambert's law, an additional contribution

$$F = -\frac{\Phi}{c} \cdot A \cos \theta \cdot \left[\frac{2}{3}\alpha e_n \right] \tag{6}$$

along the surface normal arises. The total radiation pressure force is finally obtained as

$$F = -\frac{\Phi}{c} \cdot A \cos \theta \cdot \left[(\alpha + \delta)\left(e_\odot + \frac{2}{3}e_n \right) + 2\rho \cos \theta \cdot e_n \right]. \tag{7}$$

As may be recognized from this expression, absorbed and diffusely reflected photons both result in the same net force opposite to a "weighted average" ($e_\odot + 2/3 \cdot e_n$) of the Sun direction and the surface normal. Specular reflection, in contrast, causes a net force that is strictly parallel to the surface normal. The assumption of instantaneous re-emission implies that only the sum of absorbed and diffusely reflected photons occurs in (7). As a consequence, the modeling of solar radiation pressure depends on just a single parameter (either ρ or $\alpha + \delta = 1 - \rho$).

The above equations provide the basis of box-wing-type radiation pressure models (Marquis and Krier 2000; Rodriguez-Solano et al. 2012b; Ikari et al. 2013), which describe the spacecraft by a small number of discrete surfaces (e.g., a box-shaped or cylindrical body and the solar panel "wings"). More elaborate SRP models employ finite element representations of the spacecraft structure and ray-tracing techniques to account for mutual shading as well as multiple reflections (Ziebart 2004). Corresponding models have, e.g., been developed for GPS Block IIR (Ziebart et al. 2003) and the old GLONASS II ν satellites (Ziebart and

Dare 2001), but no such models have so far been published for the latest generation of GPS Block IIF and the current GLONASS-M constellation.

To reduce the computational effort associated with the use of very detailed surface models, approximations using harmonic expansions are often employed. For GPS Block IIA and IIR satellites, such models have been derived by Fliegel et al. (1992) and Fliegel and Gallini (1996). Their T20 and T30 models provide expressions for the radiation pressure force along the x- and z-axes based on a Fourier expansion of more detailed surface force models (e.g., ROCK42) in terms of the Sun elongation ε. More recently, similar models for the BeiDou satellites have been derived by Feng et al. (2014), but no models of this kind are presently available for GLONASS, Galileo, and the Quasi-Zenith Satellite System (QZSS).

2.3 Empirical SRP models

Empirical force model parameters are commonly introduced in satellite orbit determination to compensate deficiencies in the a priori model (Wu et al. 1991). While empirical accelerations (Colombo 1989) or stochastic pulses (Beutler et al. 2006) along the principal axes of the orbital frame are well suited to isolate (or constrain) specific variations of the orbital elements, a Sun-oriented reference frame appears more suitable for the treatment of solar radiation pressure perturbations. Beutler et al. (1994) and Springer et al. (1999) have, therefore, introduced the right-handed DYB frame which is aligned with the satellite–Sun direction and the nominal solar panel axis in yaw-steering mode:

$$
\begin{aligned}
\boldsymbol{e}_D = \boldsymbol{e}_\odot \quad &= +\cos \varepsilon \cdot \boldsymbol{e}_z + \sin \varepsilon \cdot \boldsymbol{e}_x \\
\boldsymbol{e}_Y = \boldsymbol{e}_y \\
\boldsymbol{e}_B = \boldsymbol{e}_D \times \boldsymbol{e}_Y &= +\sin \varepsilon \cdot \boldsymbol{e}_z - \cos \varepsilon \cdot \boldsymbol{e}_x .
\end{aligned}
\tag{8}
$$

Within their CODE model, the empirical accelerations

$$
\begin{aligned}
a_{\mathrm{emp},D} &= D_0 + D_c \cdot \cos u + D_s \cdot \sin u \\
a_{\mathrm{emp},Y} &= Y_0 + Y_c \cdot \cos u + Y_s \cdot \sin u \\
a_{\mathrm{emp},B} &= B_0 + B_c \cdot \cos u + B_s \cdot \sin u
\end{aligned}
\tag{9}
$$

in DYB direction at 1 AU is parameterized in terms of three constant accelerations (D_0, Y_0, B_0) and up to six accelerations ($D_{c,s}$, $Y_{c,s}$, $B_{c,s}$) varying with a 1/rev periodicity. The latter refer to the argument of latitude u of the GNSS satellite, even though the orbit angle μ provides a more natural choice for the description of SRP effects. The alternative formulation

$$
\begin{aligned}
a_{\mathrm{emp},D} &= D_0 + D_c^* \cdot \cos \mu + D_s^* \cdot \sin \mu \\
a_{\mathrm{emp},Y} &= Y_0 + Y_c^* \cdot \cos \mu + Y_s^* \cdot \sin \mu \\
a_{\mathrm{emp},B} &= B_0 + B_c^* \cdot \cos \mu + B_s^* \cdot \sin \mu
\end{aligned}
\tag{10}
$$

is therefore preferable, whenever a physical interpretation of the CODE model parameters is desired. The two parameter sets are related by

$$
\begin{aligned}
B_c^* &= -B_c \cdot \cos u_\odot - B_s \cdot \sin u_\odot \\
B_s^* &= +B_c \cdot \sin u_\odot - B_s \cdot \cos u_\odot
\end{aligned}
\tag{11}
$$

and corresponding expressions for the D and Y terms, where $u_\odot$ denotes the argument of latitude of the Sun.

Even though the CODE model was originally intended for use with an analytical or semi-empirical a priori model, a good performance can also be obtained without such a priori models. A purely empirical CODE model (with 5–9 estimation parameters) has, therefore, been employed within the second IGS reprocessing campaign and is presently common practice among most IGS Analysis Centers for the routine processing of GPS and GLONASS orbits (IGS 2014). It has likewise been most widely adopted for precise orbit determination of the GIOVE-A/B and Galileo IOV satellites (Píriz et al. 2006; Schönemann et al. 2007; Steigenberger et al. 2014) due to the lack of alternative analytical SRP models.

2.4 Semi-empirical SRP models

A special variant of empirical models aims at the construction of improved a priori models from the long arc adjustment of model properties. Motivated by the T20/T30 models, the family of GPS Solar Pressure Models (GSPM) developed by the Jet Propulsion Laboratory (JPL) uses a Fourier expansion to describe the variation of the acceleration in the spacecraft system as a function of the Sun elongation (Bar-Sever and Russ 1997; Bar-Sever and Kuang 2004; Weiss et al. 2014). The Extended CODE model (ECOM; Springer et al. 1999) follows a similar approach, but combines a short (first- and third-order) harmonic expansion for the z and x acceleration in the spacecraft frame with constant accelerations in the DYB frame.

Rodriguez-Solano et al. (2012b), finally, use a box-wing representation with adjustable optical properties in combination with an empirical Y acceleration and solar panel lag angle for orbit determination of GPS and GLONASS. When combined with a proper attitude model for the eclipse phase a notable improvement of the orbit quality is demonstrated from the analysis of point positioning results and time series of geodetic parameters (Rodriguez-Solano et al. 2014). Despite this success, a prevailing problem of the adjustable box-wing model lies in the need for proper knowledge of the satellite surface areas and their optical properties, which is presently only available for GPS and, partly, GLONASS. Optimum results are only achieved with tight a priori constraints on most estimation parameters. Further investigations will, therefore, be needed to study the mutual correlation of these estimation parameters or to identify parameter

subsets and combinations that can be freely estimated if no good a priori knowledge is available.

## 3 CODE SRP modeling performance for Galileo satellites

As already mentioned in the introduction, the orbit determination of the GIOVE and Galileo IOV satellites is known to suffer from radial orbit errors with an orbital periodicity. The radial orbit errors can be evidenced through comparison of GNSS-based orbit solutions with SLR measurements. Furthermore, periodic clock variations which are highly correlated with the SLR residuals can be recognized for satellites operating a highly stable hydrogen maser.

For the purpose of illustration, the residuals of SLR measurements of Galileo IOV-2 relative to precise orbits determined by the Astronomical Institute of the University of Bern (AIUB) for the MGEX project (Prange et al. 2014) are shown in Fig. 3 (top). The diagram covers a 6-month interval during which the Sun elevation above the orbital plane varies between the extreme values of about ±65°. Aside from a mean bias of about −7 cm, the residuals show a pronounced "bow-tie" pattern. While the peak-to-peak amplitude amounts to roughly 40 cm during phases of low β-angles, it shrinks to almost one quarter of this value when the Sun attains a high angle w.r.t. the orbit plane. Since the line-of-sight vector from the station to the satellites always exhibits a small angle ($<14°$) with the radial direction for GNSS satellites in medium Earth orbit (MEO), the SLR resid-

uals can essentially be considered as a measure of the radial orbit error in the respective Galileo orbit products. Similar to most other MGEX analysis centers, the AIUB solution is based on a 5-parameter CODE SRP model (Steigenberger et al. 2014). The dependence of the radial orbit errors on the Sun elevation obviously excludes limitations in the station network or gravitational force model errors as a possible origin, and provides a first evidence of SRP modeling issues related to the empirical CODE model.

Figure 3 (bottom) illustrates the variations of the observed clock solution for Galileo IOV-2 over a 4-day period. Clock solutions from the daily AIUB MGEX product have been referred to a high-precision ground clock (H-maser at BRUX), concatenated at the day boundaries and detrended with a second-order least-squares polynomial. The resulting variations exhibit an obvious orbital periodicity (approx. 14 h) and largely match the variation of the SLR residuals in the respective time frame. For GIOVE-B, similar results have earlier been presented in Svehla et al. (2010) and Montenbruck et al. (2012). The figure illustrates the potential of high-performance GNSS satellite clocks to monitor (or even constrain; see Hackel et al. 2014) radial orbit determination errors. Compared to SLR tracking, which is often restricted to night-time observations, the clock variation can be monitored throughout the entire orbit. On the other hand, it does not provide absolute range measurements and may suffer from deficiencies such as day-boundary discontinuities and thermal clock variations.

For further investigation, plots of IOV-2 radial orbit errors vs. Sun elongation (ε) are given in Fig. 4. Both SLR residu-
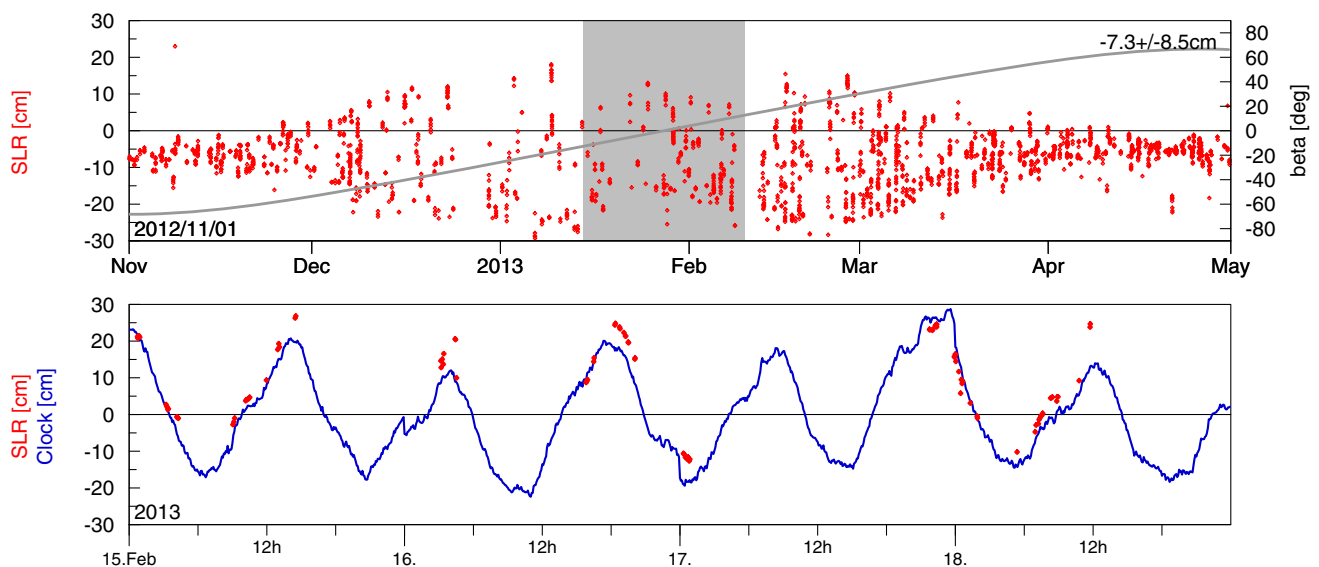

Fig. 3 Radial errors of AIUB Galileo IOV orbit determination results as evidenced by SLR residuals and periodic variations of the observed clock offset. *Top* SLR residuals of Galileo IOV-2 over a full range of Sun elevations w.r.t. the orbital plane. The β-angle is indicated by a *solid gray line* and the eclipse season is marked by the *shaded area*. *Bottom* Detrended clock offset of the Galileo IOV-2 satellite for a 4-day arc in February 2013. The observed clock offset (*solid line*) exhibits a clear 1/rev signature which correlates with the SLR residuals (*red diamonds*)
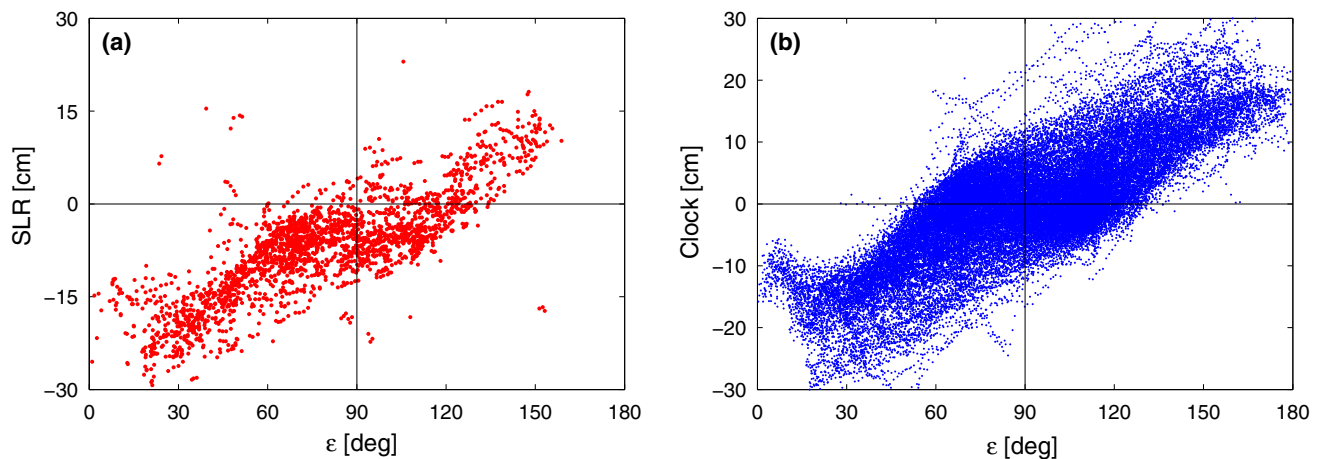
Fig. 4 Radial errors from SLR (**a**) and clock residuals (**b**) for the IOV-2 satellite based on AIUB MGEX precise orbit products for 1 November 2012 to 30 November 2013 time frame. The sign of the clock residuals has been chosen such as to evidence radial orbit errors
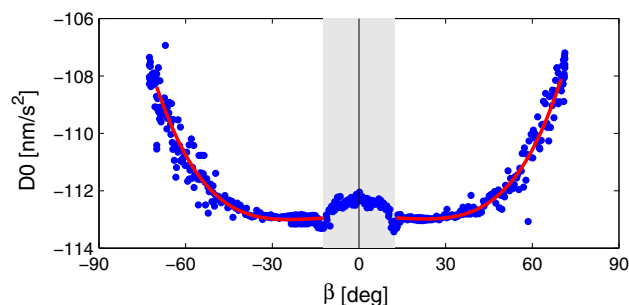
Fig. 5 Variation of estimated SRP coefficient D_0 of IOV-3 when using the 5-parameter CODE SRP model without a priori model. The *red line* represents a fourth-order polynomial fit, the *gray-shaded area* marks the eclipse season

als and clock variations data consistently evidence a unique functional relationship between the radial orbit error and the instantaneous Sun elongation, which applies for all seasons irrespective of the β-angle.

Deficiencies in the Galileo SRP modeling do not show up in radial orbit errors alone but can also be recognized from the estimated SRP parameters, when applying the 5-parameter CODE model without any a priori model. This is most obvious for the D_0 coefficient, which effectively measures the mean acceleration in (anti-)Sun direction across an orbit. As illustrated in Fig. 5, the estimated D_0 values for the IOV satellites vary by roughly 6 nm/s^2 between low and high β-angles.

As will be shown, these limitations can be overcome by combining the CODE model with a suitable a priori box model taking care of the basic properties of the spacecraft body. Other than the GPS satellites with their predominantly cubic structure, the IOV satellites resemble a telephone box with a quadratic bottom size of about 1 m × 1 m and a height of about 2.5 m (Fig. 1). At low β-angles the Sun consecutively illuminates the $+z$, $+x$, and $-z$ surfaces. For high

Sun elevations, in contrast, the satellite mainly exposes the $+x$ panel to the Sun. In this case, the effective cross section and thus the net SRP acceleration are therefore smallest. The non-cubic shape of the satellite body thus provides a natural explanation for the deficiencies of the CODE SRP model in case of the Galileo IOV spacecraft.

4 Galileo a priori SRP model

4.1 Cuboid box model formulation

The lack of accurate dimensions and optical properties for the Galileo satellites presently inhibits the development of a purely analytical box-wing model as a stand-alone SRP model for these spacecraft. An alternative approach is therefore proposed, which combines a simplified a priori box model for the spacecraft body contribution with the empirical CODE model. The resulting SRP acceleration is given by

$$\boldsymbol{a} = \frac{1\,\text{AU}^2}{r_\odot^2}\left(\boldsymbol{a}_\text{box} + \boldsymbol{a}_\text{emp}\right) \tag{12}$$

where $\boldsymbol{a}_\text{box}$ denotes the a priori model and $\boldsymbol{a}_\text{emp}$ comprises the empirical accelerations as given in (10). Both contributions are normalized to 1 AU to avoid seasonal changes induced by the varying Earth–Sun distance. No explicit solar panel contribution is considered, since the corresponding acceleration is always directed along the (negative) D-axis for nominal solar panel orientation and will thus be covered through the D_0 term of the empirical model. In addition, the empirical accelerations are expected to compensate (at least in partly) the differences between the simple box model and a more rigorous description of the body-related SRP accelerations as well as possible deviations from a nominal spacecraft atti-

tude. Other than traditional box-wing models, which sum-up the contributions of individual surface panels, the present model employs a parameterization that isolates distinct contributions (cube, cuboidness, z-asymmetry).

Confining ourselves to non-eclipse periods, where the attitude can be described by the nominal yaw-steering law (1), only the nadir facing $+z$ panel, the anti-Earth $-z$ panel and the sunlit $+x$ panel of a box-shaped spacecraft body contribute to the SRP. For the ease of notation, we introduce the characteristic accelerations

$$
\begin{aligned}
a_i^{\alpha\delta} &= \frac{\Phi_0}{mc} \cdot A_i \cdot (\alpha_i + \delta_i) \\
a_i^{\rho} &= \frac{\Phi_0}{mc} \cdot A_i \cdot \rho_i
\end{aligned}
\tag{13}
$$

related to absorption plus diffuse reflection (superscript $^{\alpha\delta}$) and reflection (superscript $^{\rho}$) of the individual body surfaces. Here, A_i with $i = \{+z, -z, +x\}$ denotes the surface area of the three panels while Φ_0 and m are the solar flux at 1 AU and the spacecraft mass. To isolate the impact of asymmetric (A) and symmetric contributions from the $+z$ and $-z$ surface, we introduce the mean value and semi-difference

$$
\begin{aligned}
a_z^{\alpha\delta} &= \frac{1}{2}(a_{+z}^{\alpha\delta} + a_{-z}^{\alpha\delta}) \quad & a_A^{\alpha\delta} &= \frac{1}{2}(a_{+z}^{\alpha\delta} - a_{-z}^{\alpha\delta}) \\
a_z^{\rho} &= \frac{1}{2}(a_{+z}^{\rho} + a_{-z}^{\rho}) \quad & a_A^{\rho} &= \frac{1}{2}(a_{+z}^{\rho} - a_{-z}^{\rho})
\end{aligned}
\tag{14}
$$

for each of these quantities. Likewise, we parameterize the SRP model in terms of the mean and semi-difference

$$
\begin{aligned}
a_C^{\alpha\delta} &= \frac{1}{2}(a_z^{\alpha\delta} + a_{+x}^{\alpha\delta}) \quad & a_S^{\alpha\delta} &= \frac{1}{2}(a_z^{\alpha\delta} - a_{+x}^{\alpha\delta}) \\
a_C^{\rho} &= \frac{1}{2}(a_z^{\rho} + a_{+x}^{\rho}) \quad & a_S^{\rho} &= \frac{1}{2}(a_z^{\rho} - a_{+x}^{\rho})
\end{aligned}
\tag{15}
$$

of the x and z contributions to separate the impact of a stretched body shape (S) from that of a cubic (C) one.

In the most general case, a total of six parameters $(a_C^{\alpha\delta}, a_S^{\alpha\delta}, a_A^{\alpha\delta}, a_C^{\rho}, a_S^{\rho}, a_A^{\rho})$ is required in this model to describe the SRP originating from a box-shaped satellite body with nominal yaw-steering orientation. Making use of (7) and summing the individual contributions, the SRP acceleration in the spacecraft frame is given by

$$
\begin{aligned}
a_{\text{box},z} = &-a_C^{\alpha\delta} \cdot \left(\left(|\cos \varepsilon| + \sin \varepsilon + \frac{2}{3} \right) \cdot \cos \varepsilon \right) \\
&- a_S^{\alpha\delta} \cdot \left(\left(|\cos \varepsilon| - \sin \varepsilon + \frac{2}{3} \right) \cdot \cos \varepsilon \right) \\
&- a_A^{\alpha\delta} \cdot \left(\frac{2}{3} |\cos \varepsilon| + \cos^2 \varepsilon \right) \\
&- 2a_C^{\rho} \cdot (|\cos \varepsilon| \cos \varepsilon) \\
&- 2a_S^{\rho} \cdot (|\cos \varepsilon| \cos \varepsilon) \\
&- 2a_A^{\rho} \cdot \left(\cos^2 \varepsilon \right)
\end{aligned}
\tag{16}
$$

and

$$
\begin{aligned}
a_{\text{box},x} = &-a_C^{\alpha\delta} \cdot \left(s \left(|\cos \varepsilon| + \sin \varepsilon + \frac{2}{3} \right) \cdot \sin \varepsilon \right) \\
&- a_S^{\alpha\delta} \cdot \left(\left(|\cos \varepsilon| - \sin \varepsilon - \frac{2}{3} \right) \cdot \sin \varepsilon \right) \\
&- a_A^{\alpha\delta} \cdot (\cos \varepsilon \sin \varepsilon) \\
&- 2a_C^{\rho} \cdot \left(\sin^2 \varepsilon \right) \\
&+ 2a_A^{\rho} \cdot \left(\sin^2 \varepsilon \right).
\end{aligned}
\tag{17}
$$

Obviously, the box model itself does not include a Y component, since the respective faces are never Sun-lit during nominal yaw-steering attitude. If present, Y accelerations can, however, be taken into account through the empirical terms of the CODE model.

For a harmonized treatment of the box and CODE contributions, it is desirable to convert the above expressions for the spacecraft body acceleration into the DYB frame. This results in

$$
\begin{aligned}
a_{\text{box},D} = &-a_C^{\alpha\delta} \cdot \left(|\cos \varepsilon| + \sin \varepsilon + \frac{2}{3} \right) \\
&- a_S^{\alpha\delta} \cdot \left(|\cos \varepsilon| - \sin \varepsilon - \frac{4}{3} \sin^2 \varepsilon + \frac{2}{3} \right) \\
&- a_A^{\alpha\delta} \cdot \left(\cos \varepsilon + \frac{2}{3} |\cos \varepsilon| \cos \varepsilon \right) \\
&- 2a_C^{\rho} \cdot \left(|\cos \varepsilon| \cos^2 \varepsilon + \sin^3 \varepsilon \right) \\
&- 2a_S^{\rho} \cdot \left(|\cos \varepsilon| \cos^2 \varepsilon - \sin^3 \varepsilon \right) \\
&- 2a_A^{\rho} \cdot (\cos^3 \varepsilon)
\end{aligned}
\tag{18}
$$

and

$$
\begin{aligned}
a_{\text{box},B} = &-\frac{4}{3} a_S^{\alpha\delta} \cdot (\cos \varepsilon \sin \varepsilon) \\
&- \frac{2}{3} a_A^{\alpha\delta} \cdot (|\cos \varepsilon| \sin \varepsilon) \\
&- 2a_C^{\rho} \cdot ((|\cos \varepsilon| - \sin \varepsilon) \cos \varepsilon \sin \varepsilon) \\
&- 2a_S^{\rho} \cdot ((|\cos \varepsilon| + \sin \varepsilon) \cos \varepsilon \sin \varepsilon) \\
&- 2a_A^{\rho} \cdot \left(\cos^2 \varepsilon \sin \varepsilon \right).
\end{aligned}
\tag{19}
$$

It may be recognized that the box acceleration at any instant depends only on the Sun elongation ε, which in turn is a function of the Sun elevation β and the orbit angle μ (cf. (2)). For each of the six independent parameters, a continuous variation of the resultant acceleration with ε or μ is obtained. Other than the ROCK and GSPM models, which employ a Fourier series expansion in ε, the acceleration in the present box model is not continuously differentiable at $\varepsilon = \pi$ due to the presence of $|\cos \varepsilon|$ terms in some of the
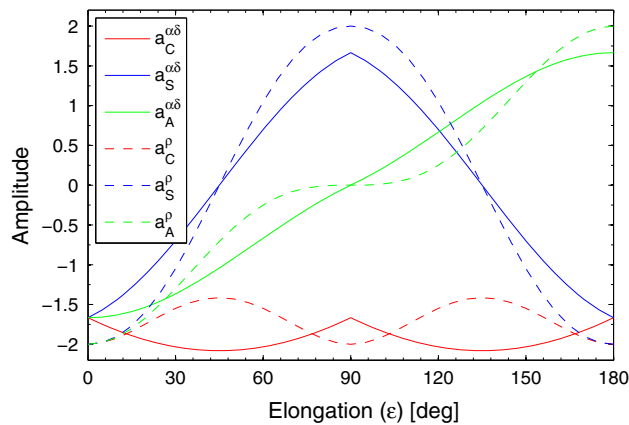
Fig. 6 Variation of SRP acceleration in the Sun direction (a_D) for unit changes in the parameters of the box model. *Colors* indicate the different constituents (*red* cube, *blue* stretch, *green* asymmetry); *solid lines* refer to absorption plus diffuse reflection and *dashed lines* to specular reflection

Table 1 Reference values of satellite body dimensions, optical properties, mass, and characteristic accelerations for the Galileo IOV satellites

Parameter	Unit	IOV
m	[kg]	700
A_x	[m^2]	1.2×1.2
A_y	[m^2]	1.2×2.5
A_z	[m^2]	2.5×1.2
$\alpha + \delta$		1.0
ρ		0.0
$a_C^{\alpha\delta} + a_C^{\rho}$	[nm/s^2]	+14.5
$a_S^{\alpha\delta} + a_S^{\rho}$	[nm/s^2]	+5.1
$a_A^{\alpha\delta} + a_A^{\rho}$	[nm/s^2]	0.0

expressions. These discontinuities in the first derivatives of the acceleration are characteristic for any SRP model built from discrete surface elements and mark the transitions from illumination to shading. They are expected to contribute to a more realistic representation of the radiation pressure than a smoothed Fourier expansion and should not be considered a deficiency of the box model.

The dependence of individual constituents of the a_D acceleration on the Sun elongation is illustrated in Fig. 6, based on which two important observations can be made. First, it may be recognized that the cube (C), stretch (S) and asymmetry (A) terms exhibit a notably different variation with ε. This "orthogonality" facilitates the separation of the individual contributions to the SRP and constitutes a major advantage of the present parameterization. Second, the figure illustrates that the specularity terms (a^{ρ}) show a similar variation with ε as the SRP accelerations due to absorption and diffuse reflection ($a^{\alpha\delta}$). Relative differences are typically confined to less than 10 %, which makes it difficult to distinguish and isolate the two contributions from the observed orbital perturbations. When developing a first-order SRP model, it is therefore legitimate to ignore the difference in optical properties and consider only lumped values ($a_C = a_C^{\alpha\delta} + a_C^{\rho}$, etc.) for the characteristic accelerations of the cube, stretch and asymmetry terms.

Considering, that $\varepsilon(\beta, \pi - \mu) = \pi - \varepsilon(\beta, \mu)$, it can be recognized that accelerations varying with $\cos \varepsilon$ exhibit a vanishing mean across the orbit. Accordingly, $a_A^{\alpha\delta}$ and a_A^{ρ} (which describe the impact of a $\pm z$ asymmetry) do not contribute to the average acceleration in D direction. Likewise, $a_C^{\alpha\delta}$ and a_C^{ρ} (which describe the SRP contribution of the cubic satellite part) as well as $a_S^{\alpha\delta}$ and a_S^{ρ} (which describe the impact of a stretched satellite body) do not contribute a mean B-acceleration.

4.2 Cuboid model parameter adjustment

Approximate values of the acceleration parameters of the Galileo IOV box model are collated in Table 1 along with the satellite properties used in their computation. In accord with the black type of thermal insulation that can be discerned from the satellite drawing (cf. Fig. 1), a specular reflection coefficient of 0.0 has been adopted. This is motivated by a corresponding value for the GPS Block IIR satellites provided in Rodriguez-Solano et al. (2012b). The main body dimensions of the Galileo IOV satellites have been extracted from Chiarini et al. (2003) and a scaled satellite model.

In view of notable uncertainties in both the box dimensions and the optical properties, the values in Table 1 exhibit an estimated uncertainty at the 10–20 % level and can only provide a coarse initial estimate of the cuboid model parameters that best represent the respective SRP accelerations. Further refinement from actual observations is, therefore, deemed necessary prior to their practical use.

Since the box model parameters cannot be estimated reliably in an orbit determination covering only a few days, a different approach has been adopted. Here, clock residuals (mapping radial orbit errors) and SRP parameter variations of CODE-only POD solutions over a full range of β-angle were employed as pseudo-observations for the box-parameter adjustment. For this purpose, orbit determination solutions have been generated at 10-day steps over a half-year interval (15 October 2013 to 13 April 2014) using Galileo IOV observations from the IGS MGEX network. With the exception of IOV-4, all IOV satellites were operated on their PHM frequency standards in this time frame. The period is specifically chosen such as to cover β-angles from $-65°$ to $+63°$ for IOV-1 and -2. In case of the IOV-3/4 satellites, which occupy a different orbital plane, β-angles between $-72°$ and $+18°$ are covered at least once during this period.

Based on the orbit determination solutions, estimated CODE model parameters ($\hat{D}_0$, $\hat{B}_0$, $\hat{B}_c^*$, $\hat{B}_s^*$) as well as the clock residuals $c\hat{\tau}$ (relative to a second-order clock polyno-
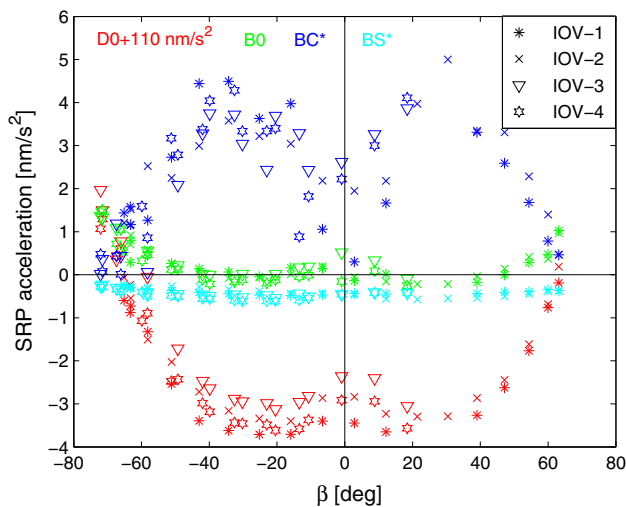
Fig. 7 Estimated CODE model parameters of the four Galileo IOV satellites without a priori box model as a function of the Sun elevation β above the orbital plane. Different CODE model parameters are indicated through *different colors*, while the indvidual satellites are distinguished by specific plot symbols
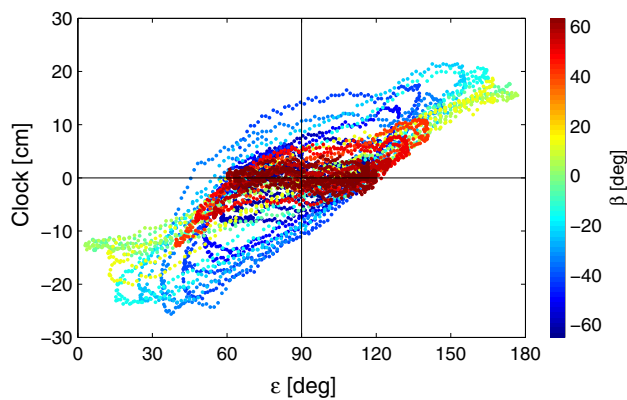
Fig. 8 Estimated clock residuals of the Galileo IOV-1 satellite as a function of the Sun elongation ε without a priori box model. Results for different β-angles are distinguished through distinct *color codes*

mial and taking into account orbit periodic relativistic corrections) were first obtained for a reference solution without a priori box model (see Figs. 7 and 8). Note that the Y-bias (Y_0) is also adjusted in the CODE model, but not considered hereafter, since the box model does not include a Y-component in nominal yaw-steering mode.

Next, six varied solutions were computed, in which a single cuboid parameter was set to a value of 10 nm/s^2, to obtain the partial derivatives

$$\frac{\partial(\hat{D}_0, \hat{B}_0, \hat{B}_c^*, \hat{B}_s^*)}{\partial(a_C^{\alpha\delta}, a_S^{\alpha\delta}, a_A^{\alpha\delta}, a_C^{\rho}, a_S^{\rho}, a_A^{\rho})} \tag{20}$$

and

$$\frac{\partial(c\hat{\tau})}{\partial(a_C^{\alpha\delta}, a_S^{\alpha\delta}, a_A^{\alpha\delta}, a_C^{\rho}, a_S^{\rho}, a_A^{\rho})} \tag{21}$$

Table 2 Modeling options for Galileo precise orbit determination (measurement model, force model, estimation parameters)
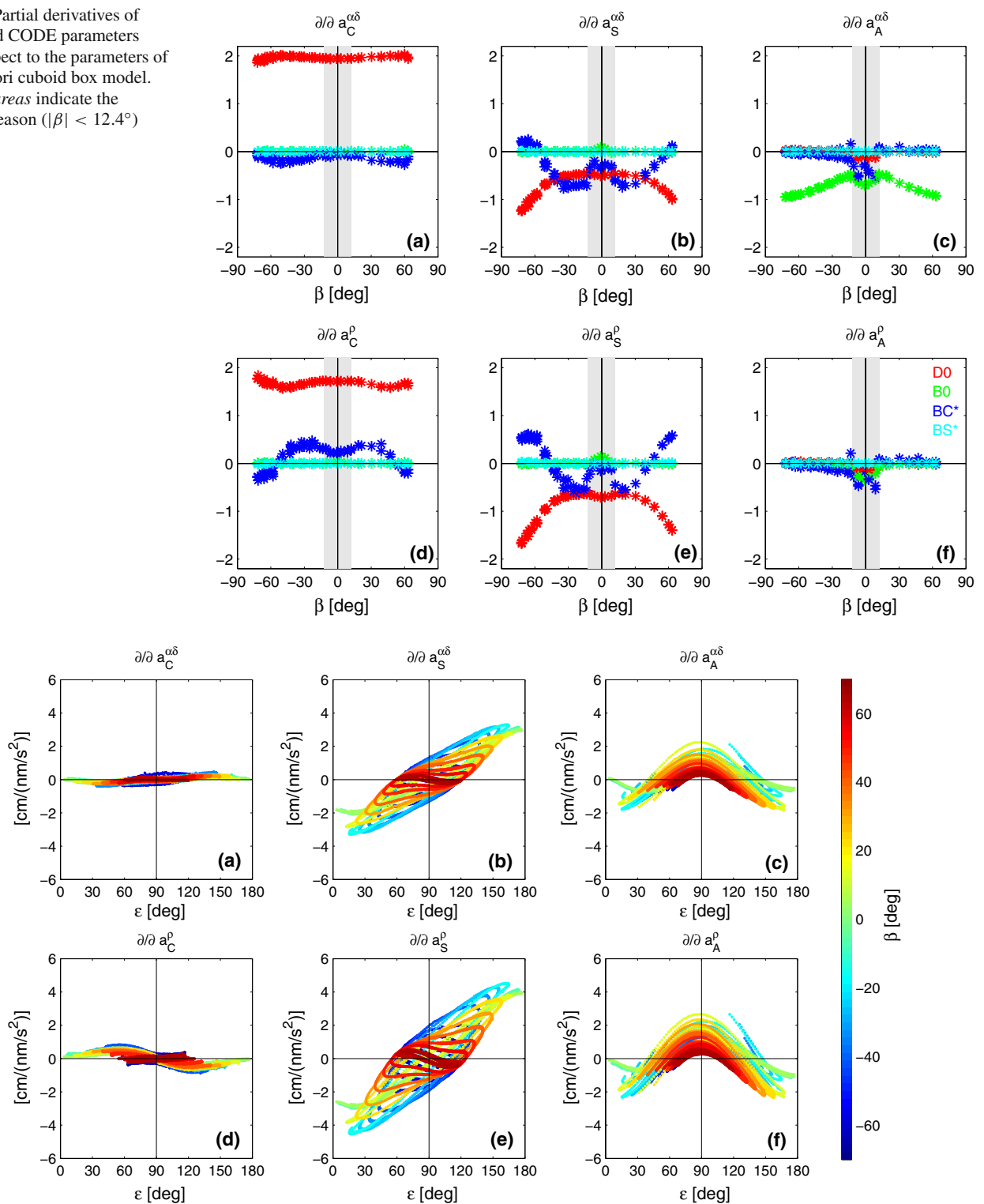
Parameter	Value
GPS stations	$\approx$100
GAL stations	$\approx$55
Observations	Undifferenced ionosphere-free code and phase combination (GPS: L1 C/A, L2 P(Y); GAL: E1 O/S, E5a)
Data arc	3 days
Sampling	5 min
Elevation cutoff	10°
Satellite antenna phase center offsets and variations	GPS: igs08.atx GAL: 0.2/0.0/0.6 m (no PCVs)
Gravitational forces	Earth, Sun/Moon/Planets (DE405), solid Earth, ocean and pole tides
Non-gravitational forces	Solar Radiation Pressure (CODE model + optional a priori cuboid box model)
	Earth albedo
Orbit	Epoch state vector
Coordinates	3 days
Tropo zenith delay	2 h
Receiver clocks	5 min
SRP parameters	D_0, Y_0, B_0, B_c, B_s
Biases	1-day ISBs, loose constraints
Earth rotation	1-day offset/drift

from a difference quotient approximation. All computations were conducted with the NAPEOS v3.3.1 software (Agueda and Zandbergen 2004), which has been modified to allow application of an a priori box model in the SRP computation next to the standard CODE model. Employed processing standards and options are collated in Table 2.

Complementary to the β and ε dependence of the estimated CODE model parameters and the clock offset residuals for the reference solution shown in Figs. 7 and 8, the corresponding partial derivatives with respect to the parameters of the a priori model are illustrated in Figs. 9 and 10. Based on these graphs the following observations and conclusions can be made:

– The CODE parameter adjustment for the IOV satellites yields a small value for the $\hat{B}_s^*$ coefficient that is essentially constant over the full range of β-angles (Fig. 7). However, the estimated values are insensitive to the choice of the a priori box model (Fig. 9a–f). They must therefore represent a different type of non-gravitational acceleration or require a more refined SRP modeling than achievable with the present cuboid box model.

Fig. 9 Partial derivatives of estimated CODE parameters with respect to the parameters of the a priori cuboid box model. *Shaded areas* indicate the eclipse season ($|\beta| < 12.4°$)

Fig. 10 Partial derivatives of clock residuals with respect to the parameters of the a priori cuboid box model

– The estimated $\hat{B}_0$ coefficients are close to zero for all β values. In view of non-vanishing partials with respect to the $a_A^{\alpha\delta}$ parameter (Fig. 9c) it can be inferred that the IOV satellites exhibit an only negligible asymmetry of the $+z$ and $-z$ panels with respect to absorption and diffuse reflection. For specular reflection (as described by a_A^{ρ}), a similar conclusion can be obtained from analysis of the clock variations (Fig. 10f). Accordingly, the two

parameters need not be taken into account in the a priori model.

- The $a_C^{\alpha\delta}$ and a_C^ρ parameters that describe the cubicness of the satellite body in the a priori model primarily affect the estimated direct solar radiation pressure coefficient $\hat{D}_0$. Their impact on this parameter is mostly independent of the β-angle (Fig. 9a, d).
- The $a_S^{\alpha\delta}$ and a_S^ρ parameters that describe the stretching (cuboidness) of the satellite body induce a characteristic β-angle dependence of the estimated $\hat{D}_0$ values (Fig. 9b, e), which closely resembles the observed variation of $\hat{D}_{0,0}$ in the absence of an a priori model (Fig. 7). Consideration of these parameters in the a priori model is therefore essential for an improved orbit modeling.
- The partial derivatives of $\hat{D}_0$ and $\hat{B}_0$ with respect to $a_C^{\alpha\delta}$ (Fig. 9a) almost match those with respect to a_C^ρ (Fig. 9d). The same consideration applies for the $a_S^{\alpha\delta}$ and a_S^ρ pair (Fig. 9b, e). It is, therefore, not practicable to separate those coefficients based on the observed β-angle variation of the estimated CODE model parameters.
- The partial derivatives of the clock variation with respect to the box model parameters (Fig. 10) yield a similar conclusion as those of $\hat{D}_0$. They can largely be explained by a cuboid contribution in the a priori model. Also, it is again difficult to discriminate the contribution of absorption and diffuse reflection (Fig. 10a–c) from that of a specular reflection (Fig. 10d–f). Accordingly, the two types of reflection need not be distinguished in the a priori model.

Based on the above considerations, we have therefore adopted an a priori box model confined to contributions from absorption plus diffuse reflection and ignoring a possible asymmetry of the $\pm z$ faces:

$$a_{\text{box},D} = -a_C^{\alpha\delta} \cdot \left(|\cos\varepsilon| + \sin\varepsilon + \frac{2}{3} \right)$$
$$- a_S^{\alpha\delta} \cdot \left(|\cos\varepsilon| - \sin\varepsilon - \frac{4}{3}\sin^2\varepsilon + \frac{2}{3} \right) \quad (22)$$
$$a_{\text{box},B} = -\frac{4}{3}a_S^{\alpha\delta} \cdot (\cos\varepsilon \sin\varepsilon).$$

This leaves just two independent parameters $a_C^{\alpha\delta}$ and $a_S^{\alpha\delta}$. The first of these is fixed to the value given in Table 1, since it is difficult to separate from the solar panel contribution. The stretching of the satellite body, in contrast, is readily observable and can be derived from a least-squares adjustment based on the observed variation of $\hat{D}_{0,0}(\beta)$ and $c\hat{\tau}(\varepsilon)$.

Estimates for each individual IOV satellite derived from both types of "observations" are collated in Table 3. Since all IOV satellites are of equal build and differ only marginally in their masses (≈ 1 %), a common value of $a_S^{\alpha\delta}$ is expected. Deviations from the mean value of 5.0 nm/s^2 amount to roughly 1 nm/s^2 for the individual satellites and the two types

Table 3 Cuboid parameter $a_S^{\alpha\delta}$ as derived from the observed variation of the $\hat{D}_{0,0}$ SRP coefficient (col. a) and the clock residuals $c\hat{\tau}$ (col. b)

Satellite	(a)	(b)
IOV-1	+6.2	+4.0
IOV-2	+5.3	+5.1
IOV-3	+4.8	+5.2
IOV-4	+4.9	(+4.4)

All values in nm/s^2. IOV-4 values in col. b are given in brackets since the satellite employed a RAFS rather than the PHM in the data analysis period

Table 4 Adopted values of the cuboid a priori model for SRP modeling of the Galileo IOV satellites

Parameter	Unit	IOV
$a_C^{\alpha\delta}$	[nm/s^2]	+14.5
$a_S^{\alpha\delta}$	[nm/s^2]	+5.0

of estimates. This scatter reflects the overall uncertainty of the parameter adjustment and provides a more realistic error estimate than formal variances of the least-squares adjustment.

5 Model validation

Based on the analysis and considerations described above, the parameters in Table 4 have been adopted for the solar radiation pressure modeling of the Galileo satellites using the a priori model in Eq. (23).

To assess the impact of the refined SRP model on the orbit quality, various types of performance metrics may be considered. Unfortunately, overlap computations did not turn out to be useful indicators of SRP model accuracy. Errors introduced in a CODE-only solution by the neglect of the box/cuboid contribution are highly correlated from one day to the next and hardly affect the overlap statistics. We, therefore, refrain from presenting overlap computations in the context of the present work but prefer to focus on more suitable performance metrics such as SLR residuals, PHM clock variations, and variability of empirical SRP parameters.

As illustrated in Fig. 11, the use of the a priori model essentially removes the β angle dependence of the estimated $\hat{D}_0$ in the CODE model. For $\hat{B}_c^*$, a constant and near-zero value would likewise be expected. However, a residual variation may still be recognized, even though its amplitude is clearly lower than for the CODE-only solution (Fig. 7). While the exact cause of the remaining $\hat{B}_c^*$ variation remains to be examined, a slightly non-nominal orientation of the spacecraft or solar panels misalignment (cf. Rodriguez-Solano et al. 2012b) may be suspected as a possible explanation.

Radial orbit errors as evidenced by SLR residuals and PHM clock variations are notably reduced when combin-
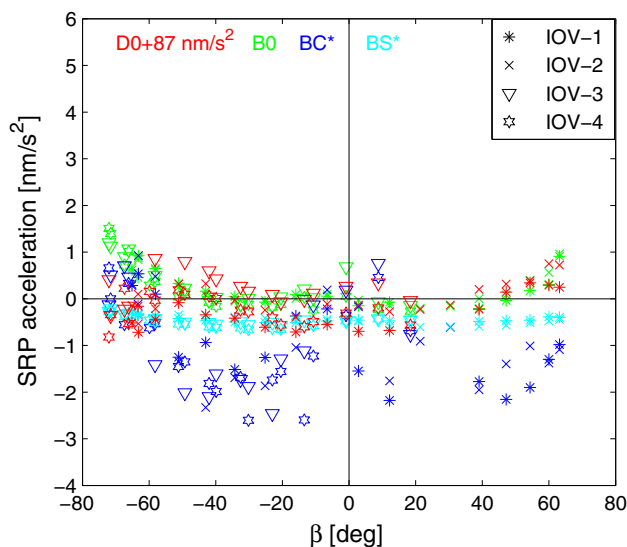
Fig. 11 Estimated CODE model parameters of the four Galileo IOV satellites with a priori box model from Table 4 as a function of the Sun elevation β above the orbital plane. Different CODE model parameters are indicated through *different colors*, while the individual satellites are distinguished by *specific plot symbols*

Table 5 SLR residuals of Galileo IOV precise orbit determination solutions computed with a CODE-only SRP model and a CODE model with a priori box contribution

Satellite	CODE-only			CODE + cuboid		
	σ	Mean	RMS	σ	Mean	RMS
IOV-1	9.35	−4.59	10.4	6.64	−3.39	7.5
IOV-2	9.84	−5.18	11.1	4.67	−2.80	5.4
IOV-3	9.38	−6.20	11.2	4.80	−2.68	5.4
IOV-4	8.05	−5.79	10.9	4.80	−2.26	5.3

All values in [cm]

ing the empirical CODE SRP model with the a priori box model established in this study. On average over the entire analysis period, the RMS values of the SLR residuals are essentially halved compared to solutions without a priori model (Table 5). Peak amplitudes, which occur close to the eclipse season at very high and very low Sun elongations are reduced from roughly 20 to 5 cm, which marks a factor-of-four improvement.

Table 5 also illustrates a remarkable reduction of the systematic SLR bias from about 6 cm down to 3 cm or less when applying the improved SRP model. As discussed before, the lacking consideration of the stretched satellite body results in systematic radial orbit errors that vary with the Sun elongation. While these errors exhibit a zero mean value across the orbit, SLR observations are more frequently collected at night-time (small ε-angles) than at day-time (large ε-angle; see Fig. 4). As a consequence of this asymmetry, negative radial errors are encountered more frequently than positive

Table 6 Clock residuals of Galileo IOV precise orbit determination solutions computed with a CODE-only SRP model and a CODE model with a priori box contribution

Satellite	CODE-only		CODE + cuboid	
	σ	σ^*	σ	σ^*
IOV-1	8.4	8.2	2.2	2.2
IOV-2	10.2	9.9	3.0	2.9
IOV-3	11.0	10.2	4.4	3.1
IOV-4	12.0	11.8	8.0	7.8

σ Denotes the standard deviation for the entire analysis period, while σ^* Refers to dates outside the eclipse period. All values in [cm]

ones and the SLR residuals of the IOV satellites exhibit a negative mean bias of several centimeters. For completeness, we note that Earth radiation pressure (ERP) is considered in the orbit computations conducted within this study. It results in an average outwards acceleration of $\Delta a \approx 1\text{nm/s}^2$ for a GNSS satellite (Rodriguez-Solano et al. 2012a) and an associated change

$$\Delta r = -\frac{1}{3}\left(\frac{T}{2\pi}\right)^2 \Delta a \tag{23}$$

of the orbital radius (at given orbital period $T \approx 14$ h) by roughly 2 cm. The magnitude of SLR biases reported in Table 5 is therefore slightly smaller than for the AIUB MGEX solutions (cf. Fig. 3), which do not account for ERP effects (Steigenberger et al. 2014; Prange et al. 2014).

According to Table 5, the GNSS-based Galileo IOV orbit determination results exhibit a residual SLR bias of about -3 cm even after consideration of ERP and the improved SRP model. This corresponds to an unmodeled acceleration of $+1.5$ nm/s^2 in radial direction and is likely to be caused by antenna thrust (Milani et al. 1987; Eanes et al. 2000). Unfortunately, details of the cumulative E1/E5ab/E6 transmit power level for the IOV satellites in the reporting period are not available. However, a power of 300 W, which is sufficient to explain the above acceleration, appears well compatible with the Galileo frequency plan and the ground-received signal strength of the publicly accessible signals.

Similar to the SLR residuals, the benefit of the refined SRP model can also be recognized in the standard deviation of the periodic clock variations. When incorporating the a priori box model to account for the cuboid contribution, the standard deviation decreases from roughly 10 cm to typically 3 cm for the IOV-1, -2, and -3 satellites, which utilized a PHM in the analysis period (Table 6). As an exception, the clock variations for IOV-4 retain a standard deviation of about 8 cm, which reflects the somewhat inferior stability of the Rubidium clock.

Since the statistics are again dominated by data obtained at medium Sun elongations (i.e., close to $\varepsilon = 90°$), the variation

of the clock residuals with Sun elongation is, furthermore, illustrated in Fig. 12. As can be recognized from comparison with Fig. 8, peak errors at very low and very high Sun elongation are reduced by roughly a factor of four from 20 to 5 cm when augmenting the empirical CODE model with the a priori box component.

The reduction of radial orbit errors at orbital time scales is of particular interest for the performance assessment of the Galileo frequency standards. Previous analyses have shown a pronounced "bump" in the Allan deviation of the hydrogen masers of GIOVE-B and Galileo (Waller et al. 2010; Montenbruck et al. 2012; Steigenberger et al. 2014), which appears incompatible with the laboratory performance and the thermal sensitivity of these clocks, but correlates strongly with radial orbit determination errors.

As shown in Fig. 13, the peak value of the Allan deviation (ADEV) at half-orbital time scales is lowered from about 7×10^{14} to less than 2×10^{14}, when combining the empirical CODE model with the a priori cuboid contribution. Following this refinement, a local ADEV maximum near one quarter of the orbital period remains for small and moderate β-angles, whereas the ADEV at high Sun elevations exhibits an almost ideal near-linear trend in the log–log representa-

tion. Further investigations will be required to understand, whether the remaining ADEV variations at low Sun elevations reflect residual orbit determination errors or have to be attributed to a thermal sensitivity of the physical oscillator and transmitter chain.

6 Summary and conclusions

Prevailing deficits in the precise orbit determination of the Galileo IOV satellites have been traced down to limitations of the CODE empirical solar radiation pressure model. While successfully applicable for present GPS satellites with a predominantly cubic spacecraft body, the stand-alone CODE model fails to properly describe the acceleration acting on a cuboid-shaped body. Use of an a priori model is, therefore, advisable to properly account for contributions of a stretched satellite body under the varying Sun illumination experienced during yaw-steering attitude control.

While box-wing or ray-tracing models are clearly desirable for solar radiation pressure modeling at the sub-nm/s^2 level, the lack of public spacecraft design data currently inhibits the construction of such models for the Galileo system. A simplified cuboid box model has, therefore, been established for these satellites and relevant parameters have been derived from coarse dimensions and a long-arc adjustment using clock residuals and CODE-only SRP parameter variations as pseudo-observations. The model employs a specific parameterization, which separates the contribution of an ideal cube from that of a cuboid and the $\pm z$ asymmetry. Compared to traditional box-wing models, this choice minimizes the correlation among individual parameters and facilitates their adjustment from observations. In addition, it is shown that specular reflection effects cannot sufficiently well be distinguished from absorption and diffuse reflection. Both constituents may thus be lumped in a first-order SRP model, which further reduces the number of independent parameters.

In view of its overall simplicity, the cuboid box model is not intended as a stand-alone model but combined with a CODE-type empirical acceleration model to account for
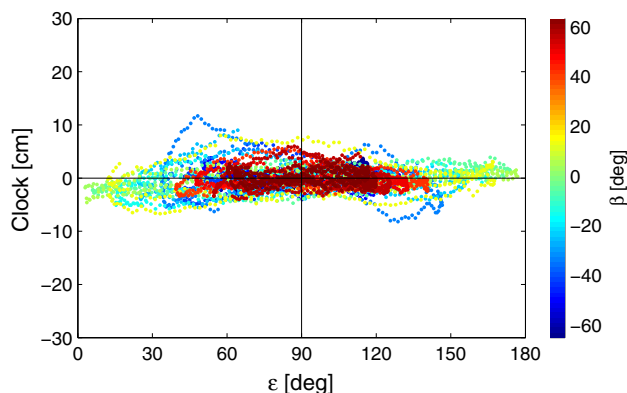
Fig. 12 Estimated clock residuals of the Galileo IOV-1 satellite as a function of the Sun elongation ε with a priori box model from Table 4. Results for different β-angles are distinguished through distinct *color codes*

Fig. 13 Allan deviation of Gallileo IOV-1 PHM from orbit determination without (**a**) and with a priori box model (**b**)
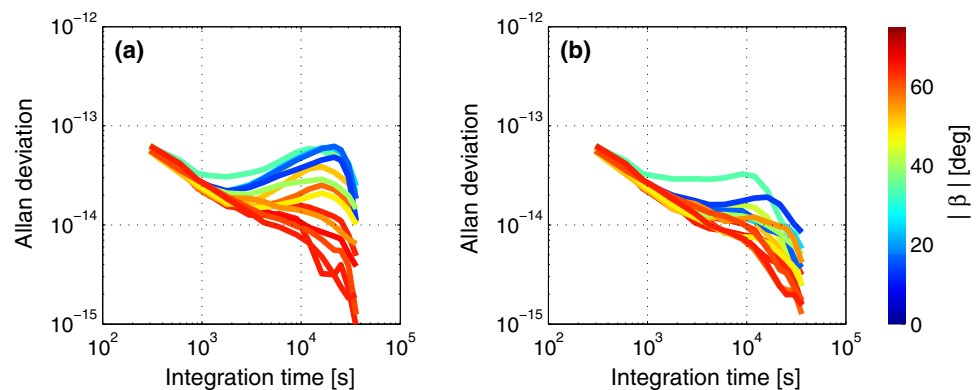
remaining unmodeled accelerations. Other than in the original CODE formulation, a parameterization of the orbit periodic accelerations in terms of the orbit angle μ (rather than the argument of latitude u) is suggested. This facilitates a physical interpretation of the estimated parameters as well as a constraining of badly observable parameters in the orbit determination process.

By augmenting the empirical CODE model with the new a priori model, significantly improved orbit solutions are obtained. For the Galileo IOV satellites, the peak amplitude of radial errors is reduced from roughly 20 to 5 cm. This marks a notable performance increase and paves the way for a more realistic assessment of the Galileo clock stability. A pronounced bump in the Allan deviation at half-orbital time scales, which has so far masked the actual performance of the passive hydrogen masers, can effectively be reduced by up to a factor of four.

While no details are known about the upcoming Full Operational Capability (FOC) satellites of the Galileo constellation, early pictures suggest a similar shape and body orientation as the IOV satellites. Use of the a priori model with IOV parameters is, therefore, considered as an initial choice for precise orbit determination of the first FOC satellites. Refined parameters can then be derived from 3 to 6 months of observations covering a suitable range of Sun elevations above the orbital plane. Besides Galileo, the presented cuboid box model appears also of interest for SRP modeling of the QZSS and BeiDou satellites, which likewise exhibit a stretched satellite body.

Despite the obvious success of the simple CODE+cuboid model for Galileo orbit determination, continued effort for the development of high-fidelity SRP models will be required to reduce the present dependence on empirical SRP parameterizations. Likewise, a proper understanding of the Galileo attitude control during shadow transits will be required for proper orbit modeling throughout the eclipse season. An increased strength of the dynamical modeling will not only enable more accurate orbit solutions, but also improve the overall contribution that Galileo can make to the realization of reference frames and geodesy in general. A public release of relevant spacecraft data for the construction of such models by the Galileo project is strongly encouraged and will greatly enhance the scientific value of this navigation system.

References

Agueda A, Zandbergen R (2004) NAPEOS mathematical models and algorithms. In: Technical Report, NAPEOS-MM-01, iss. 3.0, 04/06/2004, ESA/ESOC, Darmstadt.

Bar-Sever Y, Kuang D (2004) New empirically derived solar radiation pressure model for Global Positioning System satellites. In: Technical Report, 42–159, IPN Progress Report.

Bar-Sever YE (1996) A new model for GPS yaw attitude. J Geod 70(11):714–723. doi:10.1007/BF00867149

Bar-Sever YE, Russ KM (1997) New and improved solar radiation models for GPS satellites based on flight data. In: Technical Report, Task Plan 80–4193, Jet Propulsion Laboratory.

Beutler G (2005) Methods of Celestial Mechanics. Springer, Berlin

Beutler G, Brockmann E, Gurtner W, Hugentobler U, Mervart L, Rothacher M, Verdun A (1994) Extended orbit modeling techniques at the CODE processing center of the international GPS service for geodynamics (IGS): Theory and initial results. Manuscr Geod 19:367–386

Beutler G, Jäggi A, Hugentobler U, Mervart L (2006) Efficient satellite orbit modelling using pseudo-stochastic parameters. J Geod 80(7):353–372. doi:10.1007/s00190-006-0072-6

Binda S, Fletcher K (eds) (2011) GIOVE experimentation results: a success story. ESA SP-1320.

Chiarini JC, Smith D, Perren M, Nakache JM, Palumbo S, Gatti G, Bramante A, Emma F, Prieto RG, Alpe V et al (2003) The Galileo satellite. In: 21st International Communications Satellite Systems Conference and Exhibit, AIAA, 2003–2306, pp 1–10. doi:10.2514/6.2003-2306.

Colombo OL (1989) The dynamics of Global Positioning System orbits and the determination of precise ephemerides. J Geophys Res 94(B7):9167–9182. doi:10.1029/JB094iB07p09167

Dow JM, Neilan RE, Rizos C (2009) The International GNSS Service in a changing landscape of Global Navigation Satellite Systems. J Geod 83(3–4):191–198. doi:10.1007/s00190-008-0300-3

Eanes R, Nerem R, Abusali P, Bamford W, Key K, Ries J, Schutz B (2000) Glonass orbit determination at the Center for Space Research. In: Proceedings of the International GLONASS Experiment (IGEX-98) Workshop, IGS, Jet Propulsion Laboratory.

Feng W, Guo X, Qiu H, Zhang J, Dong K (2014) A study of analytical solar radiation pressure modeling for BeiDou navigation satellites based on raytracing method. In: China Satellite Navigation Conference (CSNC) 2014 Proceedings: Volume II, Springer, Lecture Notes in Electrical Engineering, vol 304, pp 425–435. doi:10.1007/978-3-642-54743-0_35.

Fliegel HF, Gallini TE (1996) Solar force modeling of block IIR Global Positioning System satellites. J Spacecr Rockets 33(6):863–866. doi:10.2514/3.26851

Fliegel HF, Gallini TE, Swift ER (1992) Global Positioning System radiation force model for geodetic applications. J Geophys Res 97(B1):559–568. doi:10.1029/91JB02564

Hackel S, Steigenberger P, Hugentobler U, Uhlemann M, Montenbruck O (2014) Galileo orbit determination using combined GNSS and SLR observations. GPS Solut. doi:10.1007/s10291-013-0361-5 (online first)

IGS (2014) http://acc.igs.org/reprocess2.html. Last accessed 22 Aug 2014

Ikari S, Ebinuma T, Funase R, Nakasuka S (2013) An evaluation of solar radiation pressure models for QZS-1 precise orbit determination. In: Proceedings of ION GNSS. ION, Nashville, pp 1234–1241

Konrad A, Fischer HD, Muller C, Oesterlin W (2007) Attitude and orbit control system for Galileo IOV. Autom Control Aerosp 17(1):25–30. doi:10.3182/20070625-5-FR-2916.00006

Kouba J, Héroux P (2001) Precise point positioning using IGS orbit and clock products. GPS Solut 5(2):12–28

Marquis W, Krier C (2000) Examination of the GPS block IIR solar pressure model. In: Proceedings of ION GPS. ION, Salt Lake City, pp 407–415

Milani A, Nobili AM, Farinella P (1987) Non-gravitational perturbations and satellite geodesy. Adam Hilger Ltd., Bristol

Montenbruck O, Steigenberger P, Schönemann E, Hauschild A, Hugentobler U, Dach R, Becker M (2012) Flight characterization of new generation GNSS satellite clocks. Navigation 59(4):291–302

Montenbruck O, Steigenberger P, Kirchner G (2013) GNSS satellite orbit validation using satellite laser ranging. In: Proceedings of the 18th International Workshop on Laser Ranging, Fujiyoshida

Pearlman M, Degnan J, Bosworth J (2002) The International Laser Ranging Service. Adv Space Res 30(2):125–143. doi:10.1016/S0273-1177(02)00277-6

Píriz R, Fernández V, Auz A, Tavella P, Sesia I, Cerretto G, Falcone M, Navarro D, Hahn J, González F, Tossaint M, Gandara M (2006) The Galileo System Test Bed V2 for orbit and clock modeling. In: Proceedings of ION GNSS, Fort Worth, pp 549–562

Prange L, Dach R, Lutz S, Schaer S, Jäggi A (2014) The CODE MGEX orbit and clock solution. In: Willis P (ed) IAG Potsdam 2013 Proceedings. Springer, International Association of Geodesy Symposia, accepted for publication.

Rodriguez-Solano C, Hugentobler U, Steigenberger P, Lutz S (2012a) Impact of earth radiation pressure on GPS position estimates. J Geod 86(5):309–317. doi:10.1007/s00190-011-0517-4

Rodriguez-Solano C, Hugentobler U, Steigenberger P, Bloßfeld M, Fritsche M (2014) Reducing the draconitic errors in GNSS geodetic products. J Geod 88(6):559–574. doi:10.1007/s00190-014-0704-1

Rodriguez-Solano CJ, Hugentobler U, Steigenberger P (2012) Adjustable box-wing model for solar radiation pressure impacting GPS satellites. Adv Space Res 49(7):1113–1128. doi:10.1016/j.asr.2012.01.016

Schönemann E, Springer T, Otten M, Becker M, Dow J (2007) GIOVE: a precise orbit determination from microwave and satellite laser ranging data—first perspectives for the Galileo constellation and its scientific use. In: 1st Colloquium on the Scientific and Fundamental Aspects of the Galileo Program, ESA

Springer T, Beutler G, Rothacher M (1999) A new solar radiation pressure model for GPS satellites. GPS Solut 2(3):50–62

Steigenberger P, Hugentobler U, Montenbruck O, Hauschild A (2011) Precise orbit determination of GIOVE-B based on the CONGO network. J Geod 85(6):357–365. doi:10.1007/s00190-011-0443-5

Steigenberger P, Hugentobler U, Loyer S, Perosanz F, Prange L, Dach R, Uhlemann M, Gendt G, Montenbruck O (2014) Galileo orbit and clock quality of the IGS Multi-GNSS Experiment. Adv Space Res. doi:10.1016/j.asr.2014.06.030 (online first)

Svehla D, Schönemann E, Escobar D, Springer T (2010) Complete relativistic modelling of the GIOVE-B clock parameters and its impact on POD, track-to-track ambiguity resolution and precise timing applications. In: IGS Analysis Center Workshop 2010, Newcastle

Waller P, Gonzalez F, Binda S, Sesia I, Hidalgo I, Tobias G, Tavella P (2010) The in-orbit performances of GIOVE clocks. IEEE Trans Ultrason Ferroelectr Freq Control 57(3):738–745. doi:10.1109/TUFFC.2010.1472

Weiss J, Bar-Sever Y, Bertiger W, Desai S, Garcia-Fernandez M, Haines B, Kuang D, Selle C, Sibois A, Sibthorpe A (2014) Orbit and attitude modeling at the JPL analysis center. In: IGS Workshop 2014, Pasadena

Wu SC, Yunck T, Thornton C (1991) Reduced-dynamic technique for precise orbit determination of low earth satellites. J Guid Control Dyn 14(1):24–30. doi:10.2514/3.20600

Ziebart M (2004) Generalized analytical solar radiation pressure modeling algorithm for spacecraft of complex shape. J Spacecr Rockets 41(5):840–848. doi:10.2514/1.13097

Ziebart M, Dare P (2001) Analytical solar radiation pressure modelling for GLONASS using a pixel array. J Geod 75(11):587–599. doi:10.1007/s001900000136

Ziebart M, Adhya S, Sibthorpe A, Cross P (2003) GPS block IIR non-conservative force modeling: computation and implications. In: ION GPS 2003, Portland, pp 2671–2678.